

HDO absorption spectrum above $11\,500\text{ cm}^{-1}$: Assignment and dynamics

B.A. Voronin^{a,b}, O.V. Naumenko^a, M. Carleer^c, P.-F. Coheur^c, S. Fally^c, A. Jenouvrier^d,
R.N. Tolchenov^b, A.C. Vandaele^e, J. Tennyson^{b,*}

^a Institute of Atmospheric Optics, SB, Russian Academy of Sciences, Tomsk, Russia

^b Department of Physics and Astronomy, University College London, London WC1E 6BT, UK

^c Service de Chimie Quantique et Photophysique, Université Libre de Bruxelles, Brussels, Belgium

^d Groupe de Spectrométrie Moléculaire et Atmosphérique, Reims, France

^e Institut d'Aéronomie Spatiale de Belgique, Brussels, Belgium

Received 31 January 2007; in revised form 14 March 2007

Available online 7 April 2007

Abstract

Assignment of an HDO line list extracted from a recently measured H₂O/HDO/D₂O Fourier transform absorption spectrum recorded in the $11\,600\text{--}23\,000\text{ cm}^{-1}$ region by Bach et al. (M. Bach, S. Fally, P.-F. Coheur, M. Carleer, A. Jenouvrier, A.C. Vandaele, J. Mol. Spectrosc. 232 (2005) 341–350.) is presented. More than 94% of the 3256 lines are given quantum number assignments and ascribed to line absorption by HDO; most of the remaining lines are actually due to D₂O. High accuracy variational predictions of line positions and intensities are used for the spectral assignment process. Assignments to the $\nu_1 + 5\nu_3$, $2\nu_2 + 5\nu_3$, $\nu_1 + \nu_2 + 3\nu_3$ and $\nu_1 + 6\nu_3$ bands are presented for the first time. Comparisons are made with published ICLAS spectra covering the same spectral region and suggestions made for its recalibration. The results are used to illustrate the dynamical behaviour of highly excited vibrational states of HDO and to discuss previous vibrational assignments to high lying rotation–vibration states of this system.

© 2007 Elsevier Inc. All rights reserved.

Keywords: Vibration–rotation spectroscopy; Water vapor absorption; Spectroscopic parameters; HDO

1. Introduction

Numerous studies have been performed on the HD¹⁶O high resolution vibration–rotation spectrum in the near infrared and visible spectral regions [1–11]. These provide detailed information on the energy level structure of HD¹⁶O. Among these studies are a series of the intra cavity laser absorption spectroscopy (ICLAS) measurements [2–6,8] in the spectral regions dominated by the $4\nu_3$ band at 13853.628 cm^{-1} , $\nu_2 + 4\nu_3$ at 15166.104 cm^{-1} , $\nu_2 + 3\nu_3$ at 11969.753 cm^{-1} , $5\nu_3$ at 16920.020 cm^{-1} , $2\nu_2 + 4\nu_3$ at 16456.190 cm^{-1} , $\nu_2 + 5\nu_3$ at 18208.446 cm^{-1} , and $2\nu_2 + 3\nu_3$ band at 13278.350 cm^{-1} . The $5\nu_1$ band at 12767.141 cm^{-1}

was investigated using ICLAS with a Fourier transform spectroscopy (FTS) detection scheme [9,10], while the $6\nu_3$ and $7\nu_3$ bands at 19836.882 and 22625.528 cm^{-1} , respectively, were studied for the first time by Jenouvrier et al. [7]. Finally, 11 energy levels with $J \leq 3$ belonging to the most excited vibrational state studied to date, with vibrational energy of 25140.85 cm^{-1} , were recently characterized by Theulé et al. [13] using two photon spectroscopy.

Prior to the study of Bach et al. [12] all HDO line intensities above $11\,600\text{ cm}^{-1}$ were approximate values derived from peak absorptions and scaled using *ab initio* calculated values due to Partridge and Schwenke [14,15]. Accurate HD¹⁶O line intensities are known from Toth's measurements only in the spectral range below 7700 cm^{-1} [16]. Thus the well known spectroscopic database HITRAN(2004) [17] includes HD¹⁶O absorption lines only

* Corresponding author. Fax: +44 20 7679 7145.

E-mail address: j.tennyson@ucl.ac.uk (J. Tennyson).

up to 7500 cm^{-1} . In this connection the recently reported HD^{16}O line parameters measurements [12] based on the long pathlength FTS recordings over a wide spectral range from $11\,500$ to $23\,000\text{ cm}^{-1}$ are of importance for many applications including atmospheric studies where the simultaneous measurement of HDO and H_2^{16}O columns are used to provide valuable information on water circulation [18].

The experimental determination of the spectral line parameters provides an important starting point for theoretical models of molecular absorption and emission at different wavelengths, pressures and temperatures. A first necessary step in the theoretical treatment of an experimental line list is quantum assignment of the absorption lines. This study is devoted to identification of the experimental HD^{16}O absorption lines recorded by Bach et al. [12] using high quality variational calculations based on the work of Partridge and Schwenke [14,15] combined with spectral simulation within an effective Hamiltonian approach. A comparison of the results obtained with the available literature data is given.

Some interesting features of the HD^{16}O intra-molecular dynamics are revealed by the process of spectral assignment. These and the relationship of this work to previous studies of HD^{16}O visible spectra are discussed.

The intra-molecular dynamics of the HDO molecule differs significantly from that of the parent H_2^{16}O species due to the decrease in symmetry from C_{2v} to C_s and a considerable change in harmonic frequencies. In particular, the ω_3 frequency (3887 cm^{-1}) corresponding to OH stretch is much larger than the ω_1 for the OD stretch (2823 cm^{-1}) and ω_2 for the bending vibration (1444 cm^{-1}). This results in a series of the well isolated ($00\nu_3$) vibrational states. However, the close coincidence between the ω_1 and $2\omega_2$ harmonic frequencies combined with abnormal centrifugal distortion effects gives rise to strong high-order resonance interactions in HDO, examined both in the previous ICLAS studies and the present work. The direct observation of states with the very highly excited bending modes such as (0120) and (1110) at 14565.47 and 16049.01 cm^{-1} , respectively, were reported by Naumenko and co-workers [3,6]. Here we seek confirmation that such states are reachable from the ground vibrational state, and are just not an artifact of a vibrational labelling problem.

Due to large detuning (more than 1000 cm^{-1}) between ω_3 and ω_1 harmonic frequencies of HD^{16}O , the highly excited OH stretching states represent localized states which are of particular interest for the study of bond selective chemistry [13,19]. These investigations often involve using simple models such as the Morse oscillator to reproduce the O–H bond stretching assuming that all the excitation energy is localized on the O–H bond. The use of such approaches relies heavily on correct vibrational labelling of the states under study. Here we check and re-analyze the vibrational assignment of Theulé et al. [13].

The next section gives a summary of the experiments reported by Bach et al. [12]. Section three presents our line

assignments and the resulting energy levels we determine. Section four gives an extensive comparison with previous experimental studies. Section five discusses the intra-molecular dynamics of HDO in light of our results. Finally our conclusions are summarized in section six.

2. Experimental details

HD^{16}O spectra were recorded using a high-resolution Fourier transform spectrometer (Bruker IFS120M) at 15 cm optical path difference (0.06 cm^{-1} resolution) with a path length of 600 m . The gas sample was composed of a $\text{HD}^{16}\text{O}/\text{D}_2^{16}\text{O}/\text{H}_2^{16}\text{O}$ mixture at a total pressure of 13 hPa . The HD^{16}O pressure was calculated to be 6.3 hPa , see Table 1 in Bach et al. [12] for more details. Measurements were performed from the near infrared to the visible region at 291 K . The experimental set-up is described in more detail elsewhere ([20] and references therein).

HD^{16}O lines were isolated in the spectra by removing the H_2^{16}O lines contribution, as well as the atmospheric H_2^{16}O and $^{16}\text{O}_2$ contributions (due to the absorption within the external path between the light source and the spectrometer), as explained in [12]. Briefly, the H_2^{16}O absorption lines were subtracted using a simulated spectrum generated from the H_2^{16}O Brussels–Reims (BR) database [20–22] and available at <http://www.ulb.ac.be/cpm>. The atmospheric O_2 component was similarly removed using line parameters from the HITRAN database [17]. The D_2^{16}O lines belonging to the $4\nu_1 + \nu_3$ band were identified in the region $12\,000$ – $13\,000\text{ cm}^{-1}$ but not removed due to the lack of line parameters. As discussed below some other D_2O lines were also erroneously included in the HDO line list.

Table 1
Fitted spectroscopic constants, in cm^{-1} , and dipole transition moment parameters, for the (006) and (007) vibrational states of HDO

	(006)	(007)
E_v	19836.88860(450)	22625.58085(930)
A	17.622094(680)	16.82551(220)
B	9.028960(380)	9.00563(130)
C	5.937600(310)	5.86906(110)
$A_k \times 10^3$	8.3835(280)	8.532(100)
$A_{jk} \times 10^3$	−0.6032(170)	−2.0332(931)
$A_j \times 10^4$	4.0555(190)	5.3465(970)
$\delta_k \times 10^3$	1.39783(420)	1.569(210)
$\delta_j \times 10^4$	1.4926(140)	2.3818(970)
$H_k \times 10^5$	2.0579	2.0579
$H_{jk} \times 10^7$	4.684	4.684
$h_k \times 10^5$	3.924(180)	
N_{lev}	69	40
N_{par}	10	9
RMS	0.013	0.020
μ_{1a} (D)	0.0042	0.0015
μ_{1b} (D)	0.0010	0.0004

1σ confidence intervals are given in parenthesis. Parameters without confidence intervals were fixed to those of the (005) state [5].

HD¹⁶O line parameters (positions, areas, widths) were obtained by fitting 3256 observed lines with Voigt profiles convolved with the instrument function, using Carleer's Wspectra computer package [23]. Experimental errors for the derived parameters were evaluated by considering separately the statistical errors, given line-by-line, and the systematic errors due to uncertainties in the pressure, temperature and path length. For strong ($\sigma \geq 1.0 \times 10^{-24} \text{ cm}^{-1}/(\text{mol cm}^{-2})$) and isolated lines, the uncertainty on the position and the intensity is lower than 0.003 cm^{-1} and generally lower than 5%, respectively; it reaches higher values for weaker or blended lines.

It was found in the course of the present study that the line positions reported for the $7\nu_3$ band located above 22000 cm^{-1} by Bach et al. [12] were erroneous. An updated list is available put on the Service de Chimie Quantique et Photophysique website (<http://www.ulb.ac.be/cpm>) and is used in this work. These corrected line positions are in very good agreement with those of Jenouvrier et al. [7].

An updated experimental line list has been placed in the [Supplementary material archive](#). This line list has non-HD¹⁶O and artefact lines removed, our assignments added and intensities rescaled to the HITRAN reference temperature of 296 K using the HDO partition function [24].

3. Line assignment and energy levels derivation

Most of the lines observed in [12] could be trivially assigned based on the energy levels provided by previous studies [1–11], leaving about 670 HD¹⁶O lines for further analysis. Our spectral assignment relied greatly on the variational calculation based on the Partridge–Schwenke (PS) potential energy surface (PES) and dipole moment surfaces [14,15]. The PS PES proved to be of surprisingly high accuracy in the $11500\text{--}20000 \text{ cm}^{-1}$ region with the maximum obs. – calc. deviation in the line positions analysed not exceeding 1 cm^{-1} and displaying regular variation as J and K_a increase. It is worth mentioning that similar calculations on the H₂¹⁷O and H₂¹⁸O line position became unreliable already for energies above 16000 cm^{-1} [25], where the obs. – calc. residues rise to as much as 8 cm^{-1} .

To aid the process of line identification we used a program for automatic ro-vibrational spectra assignment [26]. This program searches for the combination differences (CD) in the given spectral interval around the calculated line positions and chooses the best variant by applying pattern recognition theory. The best candidate assignment, once approved, is stored together with the corresponding averaged upper level. The program also allows one to assign single transitions not covered by CD relations by relying on agreement between the calculated and observed position and intensity. Up to three assignments to the same line are possible. The program optimally combines the performance of quick semi-automatic assignments with the ability to carefully check every proposed line identification.

Since initially the PS calculations on HD¹⁶O were only available for upper state energy levels below 20000 cm^{-1}

[14,15,27], there was a problem assigning the $19500\text{--}23000 \text{ cm}^{-1}$ region. At first this problem was partly solved by performing calculations using an effective Hamiltonian approach on the assumption that the (006) and (007) states may be considered as isolated ones, as was made in [7]. The rotational and centrifugal distortion constants of Voronina [28] were refined by fitting to observed energies using a Watson-type Hamiltonian. These values are presented in Table 1. The leading term in the transition moment expansion was chosen in order to model the line intensities and match the observed intensities, see Table 1.

This procedure allowed the (006)–(000) and (007)–(000) bands to be assigned. However, starting from $J=7$, some of the (006) and (007) energy levels appear to be perturbed by other vibrational states which causes considerable increase in the obs. – calc. residues for these levels, and, consequently, less reliable assignments. Furthermore, some of the lines observed in the high frequency end of the spectrum remained unassigned. However new HD¹⁶O calculations were subsequently provided by Tashkun [29] and by us [30], both based on the use of the PS potential energy [14] and dipole moment surfaces [15].

Our new calculations have been performed in Radau coordinates with the DVR3D program suite [31] and a large enough basis to obtain good convergence [30]. Calculations have been made for $J \leq 15$ including all levels up to 25600 cm^{-1} ; and for $J < 3$ the calculations extended up to 34000 cm^{-1} . Wave functions from these calculations were used for labelling and analysis of ro-vibrational energy levels as well as estimating rotational constants by taking expectation values of the moment of inertia tensor. These allowed us to both confirm and extend our assignments for the (006)–(000) and (007)–(000) bands, while a new band, (106)–(000) at $22454.468 \text{ cm}^{-1}$, could also be assigned. These new HD¹⁶O calculations, yielded significantly better line positions for a number of ro-vibrational bands. In particular, the averaged obs. – calc. deviation for the (015) energy levels decreased from 0.7 to 0.4 cm^{-1} . At the same time, the new calculated energies moved further, by about 0.25 and 0.30 cm^{-1} , from measured (006) and (025) energy levels, respectively. The difference between the old and new calculations clearly depends on J value, and for energy levels with $J \geq 10$ it can reach 1.5 cm^{-1} . These improvements are similar to those calculated previously, of up to 2.3 cm^{-1} in HDO line positions, as a consequence of employing a larger basis set [4].

A significant number of the new energy levels was derived from a single line and therefore not confirmed by combination differences. However, we believe that most of these assignments are safe as we rely on criteria such as a good match between observed and calculated intensities, see Fig. 1, and regular variation of the obs. – calc. residues for line positions within a band. Fig. 2 illustrates the systematic variation in obs. – calc. with J increasing. Results are shown for the J_{0J} energy levels of several

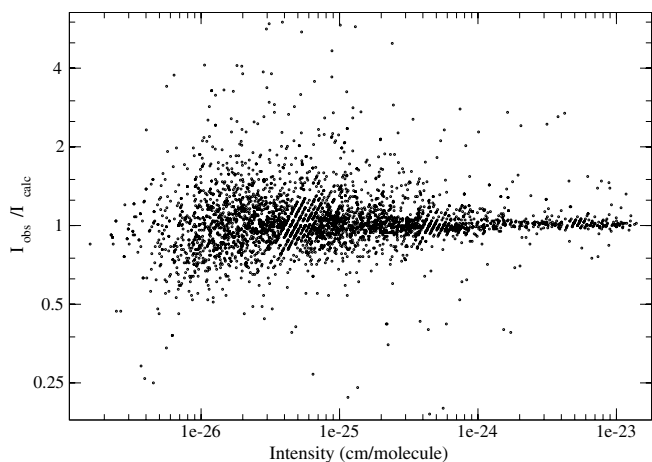


Fig. 1. Comparison of the experimental and calculated line intensities: $\frac{I_{\text{obs}}}{I_{\text{calc}}}$ intensity ratio as a function of observed line intensity.

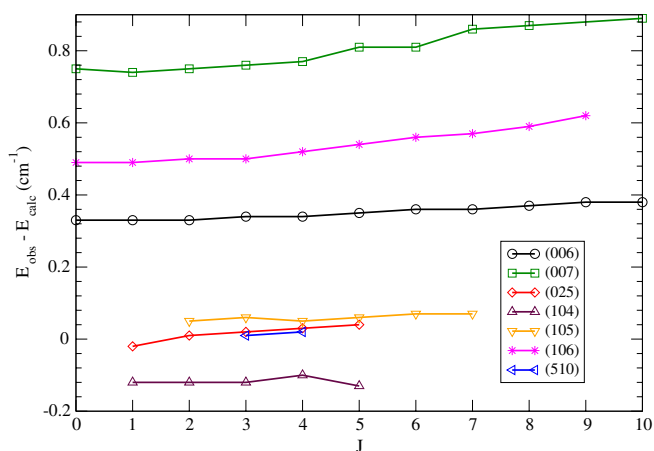


Fig. 2. Deviation of observed HDO $J_{0,J}$ energy levels as a function of rotational excitation, J .

observed vibrational bands including the highest in energy (006), (007), and (106) states.

The experimental data of Jenouvrier et al. [7] were reanalysed alongside those of Bach et al. [12], since Jenouvrier et al. left many lines unassigned. Comparison of Jenouvrier et al.'s data both with Bach et al.'s data and the H₂O line list [17] showed that of 1362 lines considered by Jenouvrier et al., 626 agree with [12], 632 are H₂¹⁶O lines and 31 are HDO lines not included in Bach et al.'s data. These were assigned as mostly (007)–(000) and (106)–(000) transitions. Finally 73 lines were left unassigned. It is probable that these lines do not belong to HDO. An updated set of HDO lines from Jenouvrier et al.'s spectrum in the 22000–22710 cm⁻¹ region which includes separate lines not observed in the spectrum [12] under study is placed in the electronic archive.

A summary of the energy levels derived in this study is given in Table 2. The total number of energy levels derived from the spectral assignment is 1370, of which 363 are reported for the first time. The set of new energy levels is presented in Tables 3 and 4. This new set consists, mainly,

of the additional levels of previously studied (006), (007), (004), and (005) states (150 levels) and those for four newly observed vibrational states: (105), (025), (113), and (106) (128 levels). The (007) and (106) energy levels derived from Jenouvrier et al.'s data [7] are marked as are the less accurate levels obtained from blended lines which have several assignments. Vibrational band origins were estimated for a number of states with an accuracy better than 0.1 cm⁻¹ from the trend in the obs. – calc. residues for the $J_{0,J}$ energy levels (see Fig. 2). These estimated band origins are also marked in Table 2. A full set of energy levels derived in this study is given in the Supplementary material. One should note that energy levels derived from the weakest FTS lines may be less accurate than those obtained from the ICLAS experiments.

As could be anticipated, we had some problems attributing ro-vibrational labels for the highly excited HD¹⁶O states due to imperfections in the automated procedure given in Ref. [14]. In trying to achieve a consistent set of labels for the levels we have relied on the previous ICLAS studies [2–6,8], although in a few cases, mostly for levels in the (023) and (103) states, we favoured the original PS labels.

About 6 percent (194 lines) of the observed transitions were left unassigned at the end of our analysis. These lines were subject to careful rechecking by calculating ratios between spectra of different HDO and D₂O relative abundances. Depending on this ratio, one can discriminate between HDO, H₂O, and D₂O; consequently a few H₂¹⁶O and some D₂O lines were eliminated from the HDO list. Moreover, the HDO lines that overlapped H₂O lines in the original experimental list (see flag in the list associated with [17]) were also removed, as well as weak unassigned lines ($\sigma < 2 \times 10^{-26}$ cm⁻¹/(mol cm⁻²)) which were treated as noise. This final list is accessible online in the Journal of Molecular Spectroscopy Supplementary material archives and on the <http://www.ulb.ac.be/cpm> website; it includes 3062 lines that correspond to 3485 transitions when unresolved doublets are taken into account. Finally integrated intensities were calculated for all assigned bands as a sum of individual line strengths. These are included in Table 2.

4. Comparison with the previous ICLAS and FTS measurements

Since much of the spectral region we consider has already been studied using ICLAS (see Table 5), a detailed comparison with the ICLAS results [2–6,8] was performed. Overall 3180 and 2572 HDO absorption lines were observed by ICLAS and FTS, respectively, in the 7 spectral regions listed in Table 5. The FTS and ICLAS sets have 2048 lines in common (defined as being within 0.035 cm⁻¹). The FTS measurements include 417 new lines compared to the ICLAS data, which, in turn, provide 1032 weak lines, not observed in FTS. Our analysis confirms the vast majority of the ICLAS assignments, and only 8 of our

Table 2
Summary of the information obtained from the assignment of the lines of Bach et al. [12]

$v_1 v_2 v_3$	Vibrational term, cm^{-1}		Lines	Levels		$I_{\text{obs.}}$	$\frac{I_{\text{obs.}}}{I_{\text{calc.}}}$	$I_{\text{obs.}}$ (a-type)	$\frac{I_a}{I_b}$
	Obs.	Calc.		All	New				
112		11315.43	1	1	0	1.35×10^{-25}	0.24	1.351×10^{-25}	
061		11533.48	4	1	0	3.17×10^{-24}	15.91	2.234×10^{-26}	0.1
410	11754.5818	11754.63	8	8	0	9.13×10^{-25}	1.73	6.947×10^{-25}	3.1
141		11804.57	18	9	0	4.10×10^{-24}	1.27	4.073×10^{-24}	126.5
330	11958.56*	11958.26	31	15	0	2.64×10^{-23}	1.17	2.564×10^{-23}	31.7
013	11969.7530	11970.07	393	138	0	7.96×10^{-22}	1.02	7.828×10^{-22}	55.6
052		12073.70	13	7	4	1.70×10^{-24}	0.24	1.677×10^{-24}	69.3
122		12644.72	1	1	1	5.24×10^{-26}	3.17	5.241×10^{-26}	
071		12694.53	4	2	2	2.84×10^{-25}	3.07	2.549×10^{-25}	8.5
500	12767.1415	12766.72	85	49	1	8.96×10^{-24}	1.09	7.614×10^{-24}	5.6
081		12852.95	3	1	1	6.04×10^{-25}	1.00	2.814×10^{-25}	0.8
023	13278.3508	13278.44	256	99	6	3.43×10^{-23}	1.02	3.181×10^{-23}	12.5
103	13331.6061	13331.74	235	75	1	1.33×10^{-23}	1.11	7.221×10^{-24}	1.1
004	13853.6280	13853.93	704	159	32	7.85×10^{-22}	1.04	7.074×10^{-22}	9.0
510	14147.43*	14147.41	7	6	6	8.54×10^{-26}	1.30	7.639×10^{-26}	8.4
033		14563.55	5	5	5	2.92×10^{-26}	1.31	2.927×10^{-26}	
0120		14565.47	24	8	1	2.68×10^{-24}	0.98	8.767×10^{-25}	0.4
113	14660.7219	14660.86	55	42	42	7.86×10^{-25}	1.20	7.866×10^{-25}	
600	15065.712	15064.98	66	34	10	8.44×10^{-25}	1.00	5.635×10^{-25}	2.0
302		15097.27	5	2	0	3.82×10^{-25}	0.96	3.192×10^{-25}	5.0
014	15166.1045	15166.53	328	123	12	5.25×10^{-23}	1.01	5.052×10^{-23}	24.6
142	15170.9510	15171.20	68	30	5	3.40×10^{-24}	0.96	2.734×10^{-24}	4.1
411		15343.05	6	2	0	1.46×10^{-25}	1.34	7.729×10^{-26}	1.1
043		15822.19	1	1	1	9.50×10^{-27}	0.91	0.000	0.0
1110		16049.01	7	3	1	9.87×10^{-26}	1.30	3.485×10^{-26}	0.5
152		16364.01	1	1	1	1.15×10^{-26}	2.19	0.000	0.0
024	16456.1903	16456.20	146	71	6	4.14×10^{-24}	0.99	4.130×10^{-24}	216.3
501		16481.89	5	3	1	5.66×10^{-26}	1.06	5.668×10^{-26}	
104	16539.04*	16539.16	43	33	11	4.08×10^{-25}	0.97	1.165×10^{-25}	0.3
005	16920.0207	16920.30	433	134	25	8.25×10^{-23}	1.00	8.049×10^{-23}	38.7
114		17844.68	2	1	0	1.80×10^{-26}	1.09	0.000	0.0
063		18202.28	5	2	1	7.89×10^{-26}	0.82	2.171×10^{-26}	0.3
015	18208.4465	18209.17	166	79	7	6.14×10^{-24}	1.08	6.136×10^{-24}	1573.2
025	19472.46*	19472.48	37	25	25	4.18×10^{-25}	0.89	4.181×10^{-25}	
105	19584.57*	19584.60	25	21	21	2.93×10^{-25}	1.05	2.932×10^{-25}	
313		19742.11	2	1	1	9.53×10^{-26}	1.57	0.000	0.0
006	19836.8828	19837.07	175	87	59	1.03×10^{-23}	0.98	1.034×10^{-23}	290.7
106	22454.4688	22453.97	38	40	40	4.13×10^{-25}	1.06	4.131×10^{-25}	
007	22625.5285	22624.78	76	51	34	1.01×10^{-24}	0.88	9.975×10^{-25}	60.4

Vibrational terms marked by ‘*’ were estimated from the obs. – calc. trend for the J_{0J} energy levels. Columns give the number of lines and energy levels associated with each vibrational band; the observed band intensity, I_{obs} in $\text{cm}^{-1}/(\text{mol cm}^{-2})$; the ratio of observed to calculated intensity; the observed intensity in a-type transitions in $\text{cm}^{-1}/(\text{mol cm}^{-2})$ and the ratio of intensity for a-type to b-type transitions (a null entry means no b-type transitions were observed for this band.)

newly derived energy levels disagree with the ones previously derived from ICLAS data.

Table 5 shows that the absolute deviation of the FTS and ICLAS line position is on average 0.010 cm^{-1} . The relative accuracy of the ICLAS HDO energy levels is better than this and may be estimated to average 0.005 cm^{-1} from combination differences. Fig. 3 presents differences between FTS and ICLAS line positions for the whole region considered. It can be seen that the ICLAS data are shifted relative to the FTS data in four spectral regions: 13 165–13 500, 16 300–16 670, 16 542–17 054, and 18 000–18 350 cm^{-1} . The ICLAS measurements in different spectral regions were calibrated using different reference lines; these calibration procedures are probably responsible for the systematic and mostly negative shifts between the FTS and ICLAS line

positions and, therefore, between the corresponding energy levels. For example, the rotational sublevels of the (103), (023), and (015) vibrational states derived in this study differ from those obtained from the ICLAS data in the 13 165–13 500 and 18 000–18 350 cm^{-1} regions by about -0.008 cm^{-1} on average, while the (024) and (005) energy levels retrieved from lines falling into 16 300–17 054 cm^{-1} spectral interval deviate from our data by -0.003 cm^{-1} . These relatively large disagreements between the FTS and ICLAS data were noted earlier [12] but without considering a possible systematic shift between two sets of data. Deviations were also found for the (500) state in the 12 600–12 850 cm^{-1} spectral region studied previously using ICLAS/FTS [10], in this case the average shift of our data from those [10] is $+0.011 \text{ cm}^{-1}$. A full comparison of our

Table 3
Newly determined energy levels, in cm^{-1} , for vibrational states of HDO

$J K_a K_c$	$v_1 v_2 v_3$	Δ	N
	052		
616	14150.2135		1
928	14554.6121	16	2
927	14630.0170		1
11110	14850.4737		1
	122		
110	12680.5131		1
	071		
110	12797.4165	16	2
212	12819.2366	53	2
	500		
110	12797.0992		1
	081		
10010	14582.5119	1	2
	023		
854	14236.1865		1
927	14110.6565		1
936	14165.8879		1
1129	14440.2243		1
12012	14302.8467 ^b		1
12111	14462.3743		1
	103		
1038	14252.5350		1
	004		
881	15123.7722		1
880	15123.7722		1
973	15096.9316		1
972	15096.9315		1
10110	14584.1322	5	3
1074	15249.0956 ^b	68	2
1073	15249.0955 ^b	70	2
1083	15411.5720		1
1082	15411.5720		1
1148	15053.9546		1
1147	15075.7222	5	2
1157	15155.9071	35	2
1156	15159.1655		1
1175	15416.5879		1
1174	15416.5881		1
12310	15131.7580		1
1249	15236.5657		1
1248	15271.0784	35	2
1257	15347.8049		1
13113	15038.7104	104	2
13311	15319.0320		1
14014	15214.0971 ^b		1
14113	15376.2223		1
14213	15376.3275		1
14312	15518.4133		1
14311	15630.7568		1
14411	15640.7882 ^b		1
15115	15401.6620		1
15114	15575.8175 ^b		1
15214	15576.9403		1
15412	15862.8947		1
16115	15787.0113 ^b		1

Δ is the experimental RMS uncertainty of level in 10^{-4} cm^{-1} and N is the number of lines used in the determination of the level. Energy levels derived from Jenouvrier et al. [7] are marked ^a. Energy levels retrieved from blended lines are marked ^b.

Table 3 (continued)

$J K_a K_c$	$v_1 v_2 v_3$	Δ	N
	510		
211	14209.9113		1
303	14231.1411		1
404	14285.0053		1
422	14356.2547		1
441	14541.3954		1
440	14541.3935		1
	033		
551	15265.7459		1
550	15265.7459		1
606	14859.8908		1
652	15358.6290		1
651	15358.6278		1
	0120		
616	15465.1237		1
	600		
211	15125.0545		1
331	15281.1967	69	2
414	15206.8611		1
441	15438.3920		1
440	15438.3901		1
514	15301.6701		1
606	15341.3570		1
616	15344.2822		1
625	15412.1961		1
717	15430.6597		1
	014		
1046	16237.8303		1
1056	16337.0450		1
1147	16416.8652		1
1156	16510.7470 ^b		1
12012	16182.5341		1
12112	16182.0626		1
12111	16334.7529 ^b		1
13013	16345.1433		1
13113	16348.0715		1
13112	16510.6686		1
14014	16520.8463		1
14114	16519.9072		1
	142		
717	15558.2575		1
11011	16037.4708		1
11111	16036.7376		1
12012	16186.7680		1
12112	16186.2909		1
	043		
1083	17897.2145		1
	1110		
212	16502.4817	3	2
	152		
707	16833.2889		1
	024		
835	17160.2980	47	2
845	17238.8875		1
844	17241.1637		1
919	17055.1675		1
918	17172.3640		1
11110	17465.5680		1
	501		
919	17054.2296		1

Table 3 (continued)

$J K_a K_c$	$v_1 v_2 v_3$	Δ	N
	104		
101	16553.9377		1
423	16735.1547		1
441	16880.0443 ^b		1
440	16880.0168 ^b		1
541	16955.8267 ^b		1
616	16826.9974		1
625	16895.2092		1
633	16967.1719 ^b		1
642	17047.2013 ^b		1
964	17614.9153		1
1056	17639.7754		1
	005		
854	17736.6745	3	2
881	18134.0987		1
880	18134.0987		1
946	17781.4884	2	2
973	18119.4478		1
972	18119.4477		1
982	18270.7378		1
981	18270.7378		1
1047	17934.4423		1
1046	17949.8688		1
1055	18030.3371	23	2
1074	18271.4439		1
1073	18271.4437		1
1138	18074.4612		1
12211	18063.4538	7	2
12210	18177.5390		1
1239	18264.0374		1
1248	18323.0862 ^b		1
1257	18391.2586		1
13013	18089.3065 ^b		1
13113	18089.3543 ^b		1
13112	18236.6145		1
13212	18236.4493		1
13311	18364.9430		1
14014	18262.5698	42	2
14114	18262.5844	52	2
	063		
303	18293.1584	26	2
	015		
11111	19062.5440		1
928	18910.2418		1
836	18868.0203	25	2
937	19003.3128		1
936	19039.8920		1
10110	18926.0272		1
1029	19048.3230		1
	313		
523	20044.3244	13	2
	006		
431	20079.2620	6	2
441	20147.2978		1
440	20147.2983	25	2
533	20154.7711	1	2
532	20157.2883	9	2
542	20223.5113	22	2
541	20223.6142		1
551	20310.7294		1
550	20310.7294		1

Table 3 (continued)

$J K_a K_c$	$v_1 v_2 v_3$	Δ	N
616	20121.4475	11	2
615	20178.9951	14	2
625	20186.0020	11	2
624	20214.9381		1
634	20245.9385	8	2
633	20252.6517	11	2
643	20315.2355	41	2
642	20315.7320	55	3
652	20402.0806	55	2
651	20402.0800	61	2
661	20507.2723		1
660	20507.2723		1
707	20210.1703	1	2
717	20210.3528	6	2
716	20281.6205	17	2
726	20285.5814	25	2
725	20328.2362	19	2
735	20351.6525	3	2
734	20365.7430	19	2
744	20422.4547	62	2
743	20424.1454		1
753	20508.9080 ^b		1
752	20508.9378 ^b		1
762	20613.8179		1
761	20613.8179		1
771	20736.2928		1
770	20736.2928		1
808	20311.0177	12	2
818	20311.2243	1	2
817	20395.2960		1
827	20399.0142		1
826	20455.2908	4	2
836	20471.3506		1
835	20496.1481	2	2
845	20545.0175		1
844	20549.5457		1
909	20423.6185	33	2
919	20423.5422	11	2
918	20520.5142		1
928	20521.0559 ^b	33	2
927	20594.6211		1
937	20604.5231		1
936	20642.6829		1
945	20692.5999		1
10010	20547.9853		1
10110	20547.9351	6	2
1019	20657.0162		1
1028	20745.1834		1
1038	20750.5436		1
11111	20684.1642		1
	007		
212	22674.8569	40	2
211	22684.2049	8	2
322	22752.2162	7	2
321	22755.7500	17	3
413	22796.6061	52	2
423	22811.0535	37	2
422	22820.3697	29	2
432	22859.8888 ^a	148	2
431	22860.6575		1
441	22923.4361		1
440	22923.4342		1
514	22874.0478	48	2

(continued on next page)

Table 3 (continued)

$J K_a K_c$	$\nu_1 \nu_2 \nu_3$	A	N
524	22883.6043	21	2
523	22901.8955		1
533	22935.7493		1
532	22938.7096		1
551	23080.0884		1
550	23080.0884		1
606	22906.2559	7	2
616	22906.5020	36	2
615	22963.8250		1
625	22969.3161		1
624	22999.4614		1
634	23026.4878		1
707	22994.3616		1
717	22994.4296		1
716	23067.7389 ^a		1
726	23067.7389		1
725	23111.3735		1
808	23094.5239		1
818	23094.0894		1
827	23178.4043		1
928	23302.7991		1
10010	23327.0822		1

newly derived energy levels with those from the available literature is presented in the [Supplementary material](#).

Table 5 shows that the averaged intensity ratio $I_{\text{FTS}}/I_{\text{ICLAS}}$ is 1.02 for all lines in common. The agreement is better (ratio near unity) for the regions labelled 2, 5, 6, and 7, than for the regions 1, 3, and 4. This can be partially explained by the fact that ICLAS line intensities were calibrated using different theoretical PS data: the most recent dipole moment surface (DMS) [15] was used for the regions 2, 5, 6, and 7 while an older and less reliable DMS [14] was used for the regions 3 and 4. No explanations could be found concerning the poor agreement of the region 1. A rescaling of the ICLAS intensities in the 11 748–12 310, 13 579–14 032, and 14 980–15 350 cm^{-1} spectral regions using the ratios evaluated from Table 5 is therefore recommended prior to any practical application or inclusion in a database.

The volume of experimental information processed in this study allows us to assess what remains to be done experimentally in the 11 500–22 700 cm^{-1} spectral region. Fig. 4 gives a comparison between the observed HDO line with the predicted lines yet to be recorded experimentally. It is seen from the figure that rather strong lines are among those still unobserved, especially in the region of the very strong (004)–(000) band at 13853.62 cm^{-1} . Some of these lines could not be detected because of unrecoverable blending with much stronger H_2O , D_2O or HDO lines, while others could not be retrieved due to insufficient experimental resolution. However, most of the undetected lines are weak and in particular many are due to the loss of sensitivity of the detector (Si diode) in the region below 14000 cm^{-1} in FTS experiments [12]. Over whole the region considered only about 430 lines are predicted to have an intensity above $2 \times 10^{-26} \text{cm}^{-1}/(\text{mol cm}^{-2})$, with about

4770 further weaker lines with intensities between 2×10^{-27} and $2 \times 10^{-26} \text{cm}^{-1}/(\text{mol cm}^{-2})$. One of the most promising regions for future experiments is 12450–12950 cm^{-1} where the unobserved but predicted and the observed HDO absorptions are of the same magnitude. The unobserved (202)–(000) band as well as many additional lines of the (500)–(000) band should be detectable in this region. Also the (203)–(000), (016)–(000), and (026)–(000) bands are the most intense still unobserved bands which may be recorded between 15 800–16 030, 20 900–21 200, and 22 200–22 450 cm^{-1} , respectively, as well as many additional lines in the (105)–(000) and (006)–(000) bands between 19 300 and 20 050 cm^{-1} .

5. The intra-molecular dynamics in HDO

5.1. Highly excited bending states

The high-order resonance interactions strengthened by close coincidence between ω_1 and $2\omega_2$ harmonic frequencies as well as abnormal centrifugal distortion effects displayed by the HDO molecule have been traced in previous ICLAS and FTS studies either serendipitously [2,4–6,8,11], or by systematic observations [3,32–35]. The local resonance interactions studied here involve highly excited bending states including (052), (152), (061), (063), (071), (081), (0120), and (1110). These states became observable through intensity stealing from stronger resonance partners. In particular, a series of $K_a = 1$ energy levels of the highest known bending states, (0120) and (1110), at 14565.47 and 16049.01 cm^{-1} , respectively, could be observed due to intensity transfer from the bright (014) and (024) states. The intensity transfer is so significant that the 24 observed transitions of the $12\nu_2$ band have an integrated intensity nearly 3 times larger than that observed for the $7\nu_3$ band based on 76 observed transitions.

Assignments to such highly excited vibrational states as (0120) and (1110) must be confirmed as the analysis is complicated by high level density and strong resonances which leads to wave functions mixing. One method of the vibrational assignment uses the assumption that the vibrational quantum number is linearly proportional to the width of a harmonic oscillator wave function [36], or, in other words, to the number of nodes in the wave function along the corresponding coordinate. However, at high vibrational excitation it is difficult to inspect properly the nodal structure of a multidimensional wave function, especially for strongly mixed states. It is therefore easier to use an automatic procedure for ascribing ro-vibrational quantum numbers such as the one used by PS [14] which is based on the analysis of the contribution of individual basis functions to the total wave function. However, for H_2O this procedure can give the same assignment to a whole set of rotational sublevels belonging to different vibrational states such as the (ν_1, ν_2, ν_3) and $(\nu_1 - 2, \nu_2, \nu_3 + 2)$ states. These states are separated by more than 700 cm^{-1} and do not interact in effective Hamiltonian representations.

Table 4
Energy levels, in cm^{-1} , for the four newly observed vibrational states of HDO

$J K_a K_c$	(1 1 3)	Δ	N	(1 0 6)	Δ	N	(0 2 5)	Δ	N	(1 0 5)	Δ	N
000	14660.7219		1	22454.4688 ^a		1						
101	14675.8118		1	22469.1679	28	2	19487.6745		1			
111	14688.8786		1	22477.7578		1	19499.4802		1			
110	14691.9900	7	2	22480.8525 ^a		1	19502.9992	88	2			
202	14705.5149	4	2	22497.8892	118	2	19517.4377		1	19628.3337		1
212	14715.9623	8	2	22504.0923		1				19635.5152		1
211	14725.2728	1	2	22513.3051		1	19536.9288	75	2	19644.4468 ^b		1
221	14764.4615		1									
220	14764.9532	10	2	22539.7066		1	19572.8733		1	19673.6209		1
303	14748.8846	19	2	22539.4449	15	2	19560.5179	6	2	19670.4467	11	2
313	14756.2947	18	2	22543.2104	32	2	19566.4552	50	2	19675.0639		1
312	14774.8520	2	2	22561.4989	45	2	19587.2995	53	2	19692.7897 ^b		1
322	14809.6470		1	22583.1164		1	19617.8470		1			
321	14811.9619	7	2				19620.9972		1	19720.1830		1
331	14883.5539		1				19685.0718		1			
330	14883.5989		1	22633.8542		1						
404	14804.9604	21	2	22592.7458	48	2	19615.7188	23	2	19724.6414	13	2
414	14809.6104		1	22594.7337	72	2	19619.2110	94	2	19727.2425		1
413	14840.2189		1	22624.6683	8	2	19653.4295		1	19756.3677		1
423	14869.5542		1	22641.3613		1				19776.0055		1
422				22649.9776		1				19783.6699 ^b		1
432	14944.8477 ^b		1									
431	14945.1535		1									
441	15049.3150		1	22762.9293		1	19837.9437		1			
440	15049.3131		1	22762.9274		1	19837.9418		1			
505	14872.7178		1	22657.4097		1	19682.3884	38	2	19790.4149		1
515	14875.2984		1	22658.3148	25	2	19684.3938		1			
514	14920.6147		1	22701.6862	81	2	19734.2077	40	2	19834.1850		1
524	14943.8623		1	22713.2784	25	2				19848.5252 ^b		1
523	14958.9133		1	22730.4622 ^a		1				19864.0870 ^b		1
532	15022.8361 ^b		1									
542	15126.3158		1	22837.7857 ^a		1	19915.3715		1			
541	15126.3177		1				19915.3553		1			
551							20028.2230		1			
550							20028.2230		1			
606	14952.3776		1	22733.3875	49	2				19867.6698		1
616	14953.7931		1	22733.8370	79	2				19868.1158 ^b		1
615	15015.0390		1	22791.0956 ^a		1	19828.3133		1			
625	15032.1403		1	22798.4263		1				19934.5509	39	2
634	15113.6792		1									
707	15043.6445		1	22820.7989 ^a		1				19956.4813		1
717	15044.3490		1	22820.9556 ^a		1						
716				22892.1782 ^a		1						
725				22938.5653		1						
808	15146.6407	1	22919.7023	1								
818	15146.9770	1	22919.8939 ^a	1								
817	15241.6129	1										
826			23063.5533 ^a	1								
909			23030.1361 ^a	1								
919			23030.0403 ^a	1								
928			23127.7363 ^a	1								

Δ is the experimental RMS uncertainty of level in 10^{-4} cm^{-1} and N is the number of lines used in the determination of the level. Energy levels derived from Jenouvrier et al. [7] are marked^a. Energy levels retrieved from blended lines are marked^b.

Such examples are much less common for the PS calculation of the HDO energy levels. We found that in the PS database the same set of ro-vibrational quantum numbers was only attached to the rotational sublevels of the (007) and (106) vibrational states at 22625.52 and 22454.46 cm^{-1} , respectively, though separate double and triple repeated assignments in the PS HDO database occur rather often for isolated levels.

We chose to investigate the vibrational identity of the (0120) and (1110) states by analysing the corresponding wave functions provided by our variational nuclear motion calculations. The vibrational energy of the (0120) state is close to that of the (033) state (14565.47 and 14563.55 cm^{-1} , respectively), suggesting a strong resonance coupling. In fact, the (012 0) and (033) wave functions, cuts through which are plotted in Fig. 5, were found

Table 5
Comparison of the FTS [12] with the ICLAS measurements of the HDO absorption spectra in the 11 748–18 350 cm^{-1} region

Region, cm^{-1}	Ref.	Band	N lines	Δ , cm^{-1}	R
1	[8]	013	1086	0.007	1.16
2	[4]	023	617	0.012	1.02
3	[2]	004	406	0.011	1.22
4	[3]	014	418	0.011	0.76
5	[6]	024	226	0.011	0.92
6	[5]	005	321	0.008	0.94
7	[6]	015	194	0.013	1.02
Total			3268	0.010	1.02

Δ is the average RMS deviation between the FTS and ICLAS line positions. R is the ratio of FTS and ICLAS summed line intensities where sum runs only over common lines.

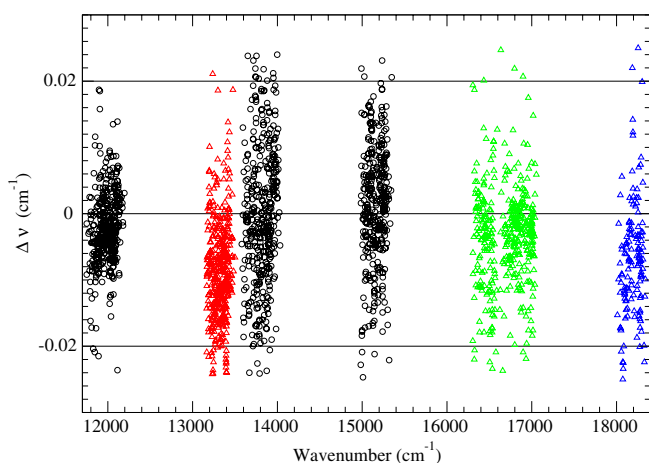


Fig. 3. Differences (in cm^{-1}) between FTS and ICLAS line positions for the whole region considered. Four regions where ICLAS data are shifted from the FTS are shown in triangles.

to be so greatly mixed that examination of their nodal structure is severely hindered.

A special procedure was therefore applied to deconvolute these wave functions, which then demonstrated clear nodal structure expected for the (0120) and (033) states (see Fig. 5). The deconvolved functions are the result of a rotation in the functional space. In the case of two mixed functions it can be written as

$$\begin{aligned}\psi'_1 &= \psi_1 \cos \gamma + \psi_2 \sin \gamma \\ \psi'_2 &= -\psi_1 \sin \gamma + \psi_2 \cos \gamma\end{aligned}$$

where ψ_1 and ψ_2 are the original mixed eigenfunctions and ψ'_1 and ψ'_2 are the deconvolved functions. A method to find γ was developed to solve the vibrational labelling problem and will be published elsewhere. For (0120) and (033) states with $J=0$, the $\cos \gamma$ was found to be 0.866. Similar investigation confirmed the vibrational assignment of the (1110) state.

In practice, only transitions involving the $K_a=1$ rotational sublevels of the (0120) state were observed in the experiment [3] due to the nature of the resonance interaction with the (014) state. These rotational sublevels are

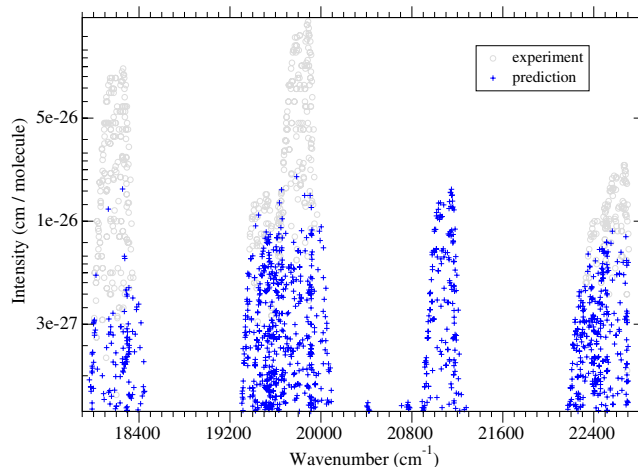
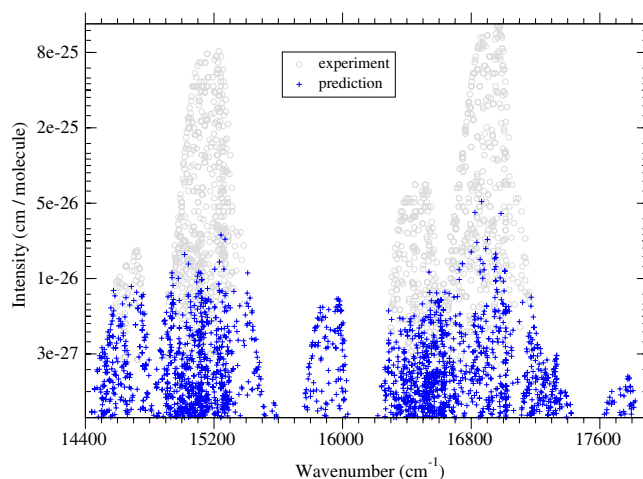
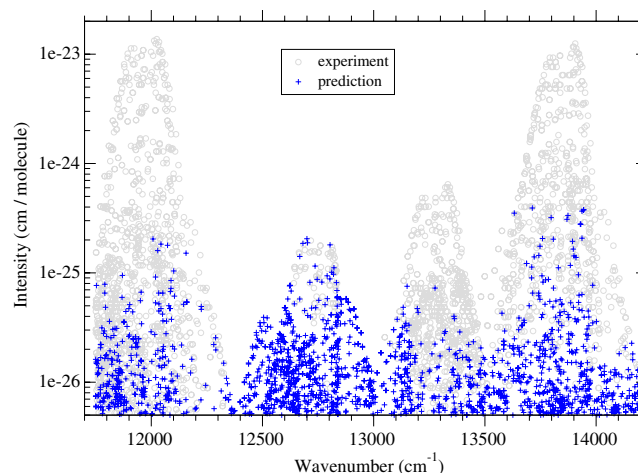


Fig. 4. Experimental [2–6,8,12] (lighter) and unobserved but predicted (darker) HDO lines in the 11 700–23 000 cm^{-1} region. Note the logarithmic scale for the intensities.

separated from the [000] (0120) state by more than 600 cm^{-1} , unlike the case of the (014) state where this separation is only about 30 cm^{-1} . It is therefore also important to inspect the wave functions of the $K_a=1$ sublevels. Fig. 6 gives a cut through the wave function of the [110] (0120) and (014) resonating states observed at

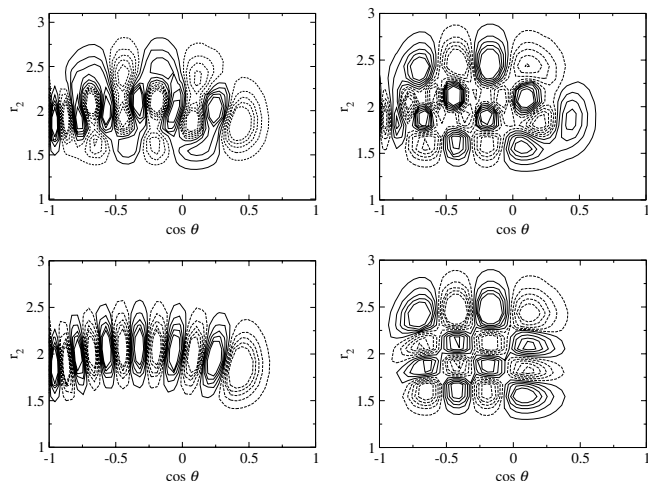


Fig. 5. The wavefunctions of (0120) (top left) and (033) (top right) states with $J = 0$. These functions can be deconvolved into the wave functions in the lower panels which have the nodal structures expected for the (0120) (left) and (033) (right). The plots are in Radau coordinates for $\cos\theta$ versus r_2 , in a_0 , and r_1 frozen at $1.77 a_0$. Solid and the dashed lines enclose regions of positive and negative amplitude, respectively.

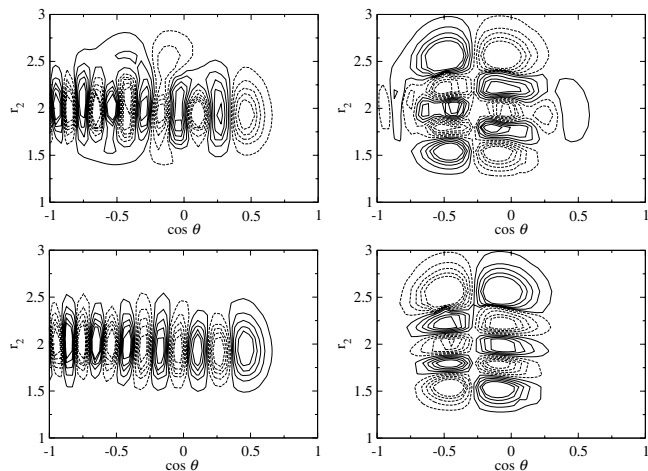


Fig. 6. The wave functions of (0120) 1_{10} (top left) and (014) 1_{10} (top right) states. The lower plots show the corresponding deconvolved wave functions. The plots are in Radau coordinates for $\cos\theta$ versus r_2 , in a_0 , and $r_1 = 1.77 a_0$. Solid and the dashed lines enclose regions of positive and negative amplitude, respectively.

15194.6746 and 15197.5800 cm^{-1} , respectively. It is evident from the figure that the wave functions are greatly mixed due to complicated resonance scheme which, in fact, involves interaction between the (014), (0120), (142), and (222) vibrational states. Again, the deconvoluted wave functions, shown in Fig. 6, demonstrate clear nodal structure typical for the (0120) and (014) states.

Fig. 7 presents the calculated (PS) and observed progressions $\frac{E_{0v_2 0}}{v_2}$, where E_{v_2} are vibrational energies of the pure bending ($0v_2 0$) states, as a function of the vibrational energy for both the H_2^{16}O and HDO molecules. Vibrational labelling of the H_2^{16}O pure bending states

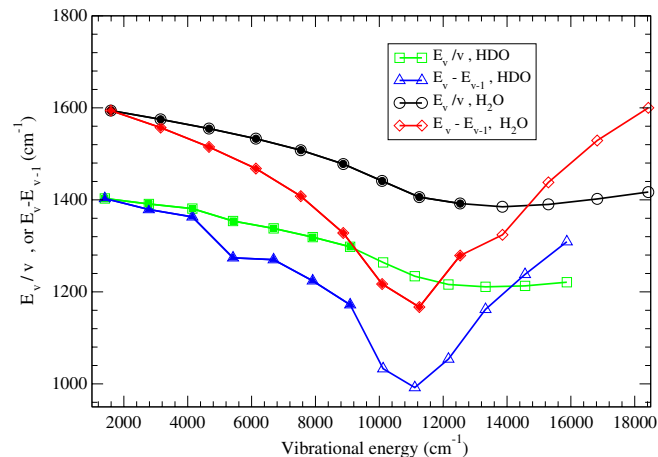


Fig. 7. Progression of $\frac{E_{0v_2 0}}{v_2}$ and $E_{v_2} - E_{v_2-1}$ shown as a function of the vibrational energy, $E_{0v_2 0}$, for the pure bending $V = (0v_2 0)$ states of the H_2^{16}O and HDO molecules. Filled symbols correspond to experimental data.

can be considered as being experimentally established at least for the first 9 states [37] and the first 15 states in many theoretical studies, see for example Refs. [14,36,38]. Fig. 7 shows that the H_2^{16}O and HDO curves are similar and both display a smooth dependence on v_2 . This, along with the very accurate predictions of the HDO band origins up to the $7v_2$ band (the maximum obs. – calc. is less than 0.1 cm^{-1}), supports the suggestion that the observed HDO state with a vibrational band origin at 14565.47 cm^{-1} corresponds to the (0120).

The calculated spacing of the energy levels $\Delta E = E_{v_2} - E_{v_2-1}$ for the ($0v_2 0$) bending progression of both H_2O and HDO is also shown in Fig. 7. The spacings decrease monotonically up to $v_2 = 8$ for H_2O and $v_2 = 9$ for HDO, which correspond to E_{v_2} values close to barrier to linearity [37]. Above these values the spacings then gradually increase. Distortions in the smooth behaviour of the curves are caused by anharmonic resonance interactions affecting the [000] energy level. It seems that the H_2O energy levels spacing is strongly perturbed only by the (090)–(160) resonance [38] at 12533 cm^{-1} , while the HDO energy levels pattern is distorted for the (050), (060), and (070) bending states by resonances with the (210), (300), and (310) states, respectively. These resonances cause considerable intensity transfer to otherwise very weak transitions to these highly excited bending states which have been observed in several experimental studies [32–35] allowing, for example, the determination of 55 levels of the (070) state from ICLAS data by Naumenko et al. [35]. In H_2O the (050), (060), and (070) states are less perturbed, leading to reduced intensity stealing. Thus only a few transitions to these states have been identified in room temperature spectra [39]. Hot emission spectra have proved to be a more fruitful source of information on the excited bending states of H_2O [37,40].

5.2. High stretching overtones in HDO

The highest vibrational state of HDO so far observed is the (008) OH overtone stretching at 25140.85 cm^{-1} [13]. In contrast to H_2O , where tunnelling between two nearly degenerate O–H stretches complicates the analysis, the OH overtone vibrations in HDO may be described using simple physical models. Thus Theulé et al. [13] constructed a quantitative model to describe the evolution of the dipole moment as the O–H bond is excited. A Morse oscillator was used to represent the O–H stretching motion assuming that all excitation was localized on O–H bond, and the remainder of molecule was accounted for parametrically. However, Bertseva et al. [5] had already demonstrated that a simple two-parameter model based on the Morse oscillator has difficulty reproducing and predicting HDO vibrational energies for $(00v_3)$ states even for $v_3 \leq 5$.

We attempted to fit the vibrational energies of the $(00v_3)$ states with $v_3 \leq 7$ to a Morse oscillator. We obtained an RMS deviation of 11.8 cm^{-1} , with the largest obs. – calc., a deviation of 13.8 cm^{-1} , for the (007) state. This model predicts that the band origin of the (008) state lies at 25218.2 cm^{-1} . Tests on the predictive ability of this two-parameter model, based on fits including all states up to $(00v_3)$, show that the $(00v_3 + 1)$ state is predicted systematically below its observed value. This led us to question whether the state observed by Theulé et al. [13] at 25140.85 cm^{-1} really correspond to 8 O–H stretches excitations. Inspecting our calculated wave function for the state in question clearly shows that the state at 25140.85 cm^{-1} is actually the (107) state. Our calculations place the real (008) state at 25330.23 . Fig. 8 shows cut through the wave functions of the (107), (008), (007), and (106) vibrational states. A clear minimum is found along the r_1 coordinate for the states we label (106) and (107), whereas those we label (008) and (007) have 8 and 7 nodes, respectively,

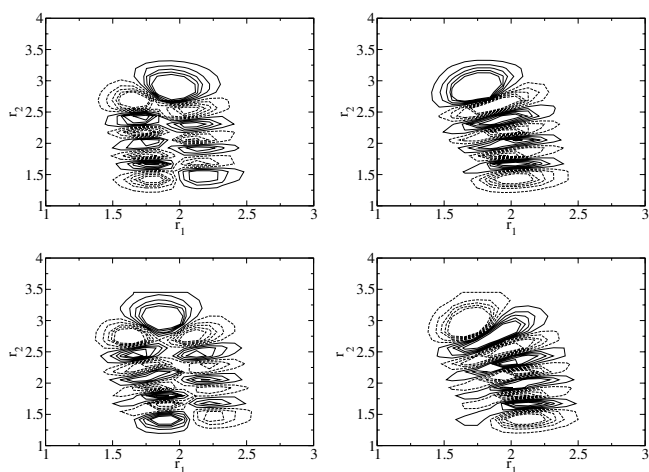


Fig. 8. The wave functions of highly excited stretch modes: top left (106), top right (007), bottom left (107), and bottom right (008). Axes are the Radau stretching coordinates r_1 and r_2 in a_0 . Cuts are for the Radau angle $\cos \theta = -0.225$. Solid and the dashed lines enclose regions of positive and negative amplitude, respectively.

along their r_2 coordinate. Our attempt to fit all the $(00v_3)$ vibrational energies up to $v_3 = 8$ using the two-parameter model yielded an RMS of 29.6 cm^{-1} , indicating that the Morse oscillator model is not appropriate for describing highly excited OH overtone vibrations in HDO molecule.

Fig. 9 shows the energy level spacing $\Delta E = E_v - E_{v-1}$ for the $(v00)$, $(00v)$, and $(10v)$ vibrational states of HDO, and the $(00v)$ and $(v,0)^{\pm 0}$ (in local mode notation) states of H_2O as a function of the vibrational energy. The figure demonstrates that our assignment for the (107) and (008) HDO states does not distort the smooth character of the $(00v)$ and $(10v)$ HDO curves, whereas the previous assignment [13] gives an $(00v)$ HDO curve which suggests that the (008) state is strongly perturbed. This is not the case since all the observed energy levels in [13] are well reproduced by a model for an isolated state. Interestingly, the $(00v_3)$ HDO progression nearly coincides with that for the local mode pairs in the H_2O molecule up to $v = 5$ for ΔE and up to $v = 7$ in vibrational energy attached to the same v quanta. This is a reflection of the fact that both curves correspond to the states in which all the excitation energy is localized in one O–H bond with ω_3 in HDO being close to $\omega = \frac{(\omega_1 + \omega_3)}{2}$ for the localized H_2O states.

Since the well separated $(00v_3)$ vibrational states represent an attractive subject for bond selective overtone spectroscopy [19], we present information here on some highly excited $(00v_3)$ states which may be useful for future studies. These are the (008), (009), and (0010) vibrational states predicted at 25330.23 , 27967.18 , and 30540.17 cm^{-1} , respectively. The identity of these states was confirmed both by inspecting their wave functions, and by the fitting their rotational energy levels up to $J = 2$ to Watson-type Hamiltonian as those of an isolated state. In all cases, adjusting the A , B , and C parameters yielded an RMS deviation of the order 0.01 cm^{-1} , confirming that indeed all the

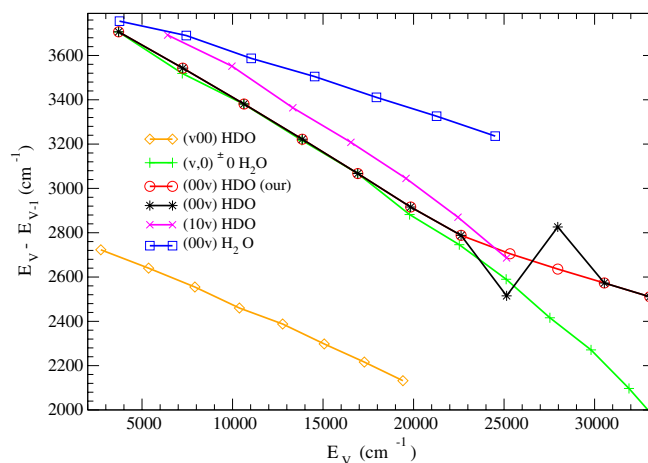


Fig. 9. Energy level spacing, $\Delta E = E(v) - E(v - 1)$, for the states $(v00)$, $(00v)$, and $(10v)$ of HDO, and $(00v)$ and $(v,0)^{\pm 0}$ (in local mode notation) of H_2O as a function of the vibrational $E(v)$ energy of the upper state.

Table 6

Spectroscopic constants, in cm^{-1} , determined by fits to the calculated energy levels with $J=0, 1$, and 2 for the (008), (009), and (0010) vibrational states of HDO and from the fitting to observed energy levels [13] for the (107) state

	(107)	(008)	(009)	(0010)
E_V	25140.85	25330.23	27967.18	30540.17
A	16.7506(140)	16.2596(20)	15.7151(10)	15.2342(20)
B	8.93445(270)	8.9288(30)	8.8498(10)	8.7628(30)
C	5.74579(220)	5.8049(30)	5.7448(10)	5.6862(20)
$A_k \times 10^3$	8.532	8.532	8.532	8.532
$A_{jk} \times 10^3$	-8.06(230)	-2.0332	-2.0332	-2.0332
$A_j \times 10^4$	5.3465	5.3465	5.3465	5.3465
$\delta_k \times 10^3$	1.569	1.569	1.569	1.569
$\delta_j \times 10^4$	2.3818	2.3818	2.3818	2.3818
$H_k \times 10^5$	2.0579	2.0579	2.0579	2.0579
$H_{jk} \times 10^7$	4.684	4.684	4.684	4.684
N_{lev}	11	9	9	9
N_{par}	4	3	3	3
RMS, cm^{-1}	1.6×10^{-2}	1.2×10^{-2}	6.0×10^{-3}	1.0×10^{-2}

1σ confidence intervals are given in parenthesis, parameters without confidence intervals are fixed to the (007) values of Table 1.

states are well isolated ones for small J values. This is typical for high overtone ($00v_3$) states of HDO. Rotational constants for the (107), (008), (009), and (0010) states are given in Table 6.

5.3. Perturbations of calculated intensities

The variational calculations, which we actively used for the identification of the observed ro-vibrational spectra, do not require a knowledge of resonance interactions as they are implicitly included in the calculations. However the investigation of possible resonance couplings between observed states is important for interpreting strong intensity perturbations for transitions to states in close resonance, particularly as these can be difficult for variational treatments to reproduce accurately.

Intensity perturbations by several orders of magnitude can occur for HDO when interacting levels coincide within 1 cm^{-1} [8]. Such close resonances are difficult to predict theoretically as they put great stress on the accuracy of the underlying potential energy surface. Accurate experimental intensities, such as those available in this study, provide an opportunity to study intensity redistribution

between lines involving resonance partners. Table 7 presents our observed and calculated intensities for transitions involving interacting energy levels. It can be seen from the table that transition intensities in the (004)–(000) band are underestimated by nearly the same values as the corresponding transition intensities in the (052)–(000) band are overestimated, as the perturbations have an equally strong influence on transitions to both states. The second example given in Table 7 illustrates resonance interactions between states for which transitions from the ground state are strong (‘bright’) and very weak (‘dark’). In this case the calculated perturbation in the intensity of the stronger transitions may be within experimental accuracy (about 5% for our data), while the intensities of weaker transitions change dramatically.

The agreement between calculated and observed intensities is significantly worse for the transitions to interacting states such as those in Table 7. Intensities predicted using variational nuclear motion calculations for such transitions are crucially dependent on having wave functions with the correct degree of mixing. This, in turn, relies on good convergence for the nuclear motion calculations and, even more importantly, on the accuracy of the underlying potential energy.

These perturbations probably influence a large number of transitions, some of which will be very strong. This should be remembered when using synthetic HDO line list. Thus, for example, the whole (330)–(000) band consisting of 31 lines is greatly perturbed due to resonance coupling with the (013)–(000) band with half of line intensities being strongly underestimated, while the other half-overestimated to nearly the same extent, yielding a good average $\frac{I_{\text{obs.}}}{I_{\text{calc.}}}$ ratio of 1.17, see Table 2. Fig. 10 shows observed to calculated intensity ratios for mostly unperturbed (005)–(000) band and for highly perturbed (330)–(000) band. However, for all the strongest bands, the correspondence between the calculated and observed intensities (Table 2 and the Supplementary material) is generally very good. Indeed we find $\frac{I_{\text{obs.}}}{I_{\text{calc.}}} = 1.02$ for the whole spectrum.

5.4. Orientation of the dipole in HDO transitions

In accordance with its C_s symmetry, both a and b-type ro-vibrational transitions are permitted for HDO. The

Table 7

Examples of intensity stealing between transitions to interacting upper states

$J'K'_aK'_c$	$J''K''_aK''_c$	$\omega_{\text{obs.}}/\text{cm}^{-1}$	$I_{\text{calc.}}$	$I_{\text{obs.}}$	$I_{\text{obs.}} - I_{\text{calc.}}$	$\omega_{\text{obs.}}/\text{cm}^{-1}$	$I_{\text{calc.}}$	$I_{\text{obs.}}$	$I_{\text{obs.}} - I_{\text{calc.}}$
		(004)				(052)			
312	413	13781.8415	5.24×10^{-24}	7.30×10^{-24}	2.06×10^{-24}	13781.3125	2.34×10^{-24}	4.47×10^{-25}	-1.89×10^{-24}
312	313	13864.4337	1.17×10^{-24}	1.61×10^{-24}	4.40×10^{-25}	13863.9051	5.24×10^{-25}	1.15×10^{-25}	-4.09×10^{-25}
312	211	13898.6403	6.45×10^{-24}	8.97×10^{-24}	2.52×10^{-24}	13898.1108	2.86×10^{-24}	5.61×10^{-25}	-2.30×10^{-24}
$J'K'_aK'_c$	$J''K''_aK''_c$	$\omega_{\text{obs.}}/\text{cm}^{-1}$	$I_{\text{calc.}}$	$I_{\text{obs.}}$	$\frac{I_{\text{obs.}}}{I_{\text{calc.}}}$	$\omega_{\text{obs.}}/\text{cm}^{-1}$	$I_{\text{calc.}}$	$I_{\text{obs.}}$	$\frac{I_{\text{obs.}}}{I_{\text{calc.}}}$
		(013)				(330)			
111	212	11939.5929	6.45×10^{-24}	6.28×10^{-24}	1.03	11941.9326	2.10×10^{-25}	1.14×10^{-25}	0.54
111	110	11965.2234	7.26×10^{-24}	7.02×10^{-24}	1.03	11967.5667	2.34×10^{-25}	6.42×10^{-26}	0.27

Intensities are given in $\text{cm}^{-1}/(\text{mol cm}^{-2})$.

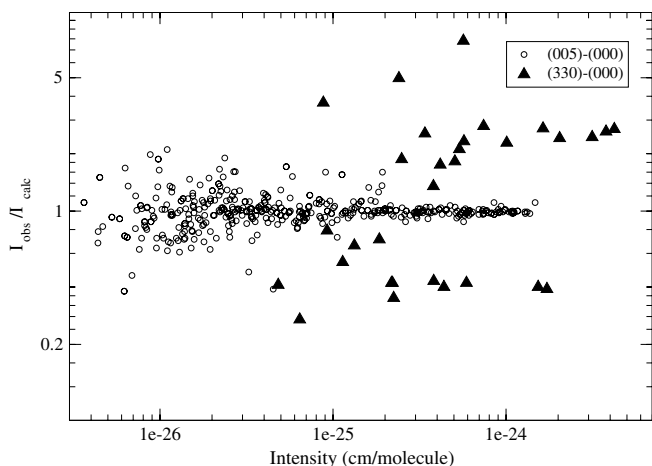


Fig. 10. Ratio of observed to calculated line intensities for largely unperturbed (005)–(000) band and for highly perturbed (330)–(000) band.

ratio of a–b-type transition intensities indicates whether the vibrational band has hybrid character or is of pure a or b-type. This ratio, in turn, depends on the orientation of the transition moment vector relative the molecular *a* and *b* axes, and is very sensitive to the quality of the dipole moment surface [41]. The excitation of OH stretches in the v_3 sequence leads to an increasing a-type character for the corresponding bands; conversely for the v_1 sequence of OD stretches the bands change from pure a character to pronounced hybrid type as v_1 increases [5,41]. Our results, shown in Table 2, confirm this finding, although the I_a/I_b ratios, which are given only for observed transitions, differ from those given by Bertseva et al. [5], where calculated a and b-type intensities were used. In practise experimental I_a/I_b ratios tend to be overestimated for bands with predominantly a-type transitions since many weak b-type transitions are too weak to be observed. Table 2 shows that for the 14 observed bands containing more than 40 transitions, only the (103)–(000), (600)–(000), and (104)–(000) bands have a pronounced hybrid character, all other bands being predominantly a-type. At the same time, resonance induced transitions to upper states with high bending excitation ($v_2 \geq 5$), are in most cases b-type or hybrid.

6. Conclusion

An HDO line list determined from high-resolution Fourier transform spectra of the H₂O:HDO:D₂O mixtures recorded in a wide spectral region (11 600–22 800 cm⁻¹) is analysed using high-accuracy variational calculations. The resulting assigned line list contains 3485 transitions (including blends) and has the experimental line intensities transformed from the 291 to 296 K. For degenerate lines, the experimental intensity is distributed between the components of the multiplet in proportion to the calculated intensities of the line components. 1370 upper energy levels are derived in the study, 363 of them being reported for the

first time. Four new weak vibrational bands; (105), (025), (113), and (106) were identified yielding 128 new energy levels.

Comparison with the previous ICLAS and FTS studies in the same spectral region reveal frequency calibration problems in some of those studies of between 0.012 and 0.003 cm⁻¹. Of the 2240 energy levels derived in these previous studies, 1006 are in common with ours. Thus the most complete set of energy levels for the HDO molecule must be constructed by merging these data, but should first allow for the appropriate recalibration of the previous measurements. Comparison of our calculated line list with the available experimental studies for the 11 700–22 800 cm⁻¹ spectral region points to a number of key regions which should be considered for further, more detailed, experimental studies.

The intra-molecular dynamics of the HDO is discussed using the extensive information on HDO energy levels and the newly available, accurate experimental line intensities. Numerous examples of intensity stealing and calculated intensities perturbations due to high-order resonance interactions are encountered. Our results support the vibrational labelling for the (0120), the highest HDO bending state observed. Conversely our analysis strongly suggests that the vibrational state which was observed recently at 25140.85 cm⁻¹ [13] and labelled (008) is actually the (107) state. This re-labelling may have consequence for the other results reported by Theulé et al. [13].

Integrated experimental intensities are provided for the vibrational bands considered. This information will be valuable for improvement of the dipole moment surface of the HDO molecule. The new extended set of the precise energy levels obtained in this study can be of great use for further optimization of the HDO potential energy surface, since rather large observed minus calculated values of up to 0.9 cm⁻¹ were found for line positions calculated using the existing potential by Partridge and Schwenke [14].

Acknowledgments

This work was jointly supported by a collaborative project between CNRS and RFBR (PICS Grant 05-05-22001) and the UK NERC, as well as by INTAS foundation. B. Voronin acknowledges the financial support from EC program FP6, Marie Curie Incoming Fellowships, Grant WWLC008535. O. Naumenko thanks support from the Royal Society of the UK. Belgian financial support by the “Actions de Recherche Concertées” (Communauté Française de Belgique), by the Federal Science Policy Office (contract SD/AT/01A), and by the “Fonds National de la Recherche Scientifique” (Fonds de la Recherche Fondamentale Collective) is also acknowledged. The study was performed as part of IUPAC task group 2004-035-1-100 on a database of water transitions from experiment and theory.

Appendix A. Supplementary data

Supplementary data for this article are available on ScienceDirect (www.sciencedirect.com) and as part of the Ohio State University Molecular Spectroscopy Archives (http://msa.lib.ohio-state.edu/jmsa_hp.htm).

References

- [1] A.D. Bykov, V.A. Kapitanov, O.V. Naumenko, T.M. Petrova, V.I. Serdyukov, L.N. Sinita, *J. Mol. Spectrosc.* 153 (1992) 197–207.
- [2] O. Naumenko, E. Bertseva, A. Campargue, *J. Mol. Spectrosc.* 197 (1999) 122–132.
- [3] O. Naumenko, A. Campargue, *J. Mol. Spectrosc.* 199 (2000) 59–72.
- [4] O. Naumenko, E. Bertseva, A. Campargue, D.W. Schwenke, *J. Mol. Spectrosc.* 201 (2000) 297–309.
- [5] E. Bertseva, O. Naumenko, A. Campargue, *J. Mol. Spectrosc.* 203 (2000) 28–36.
- [6] A. Campargue, E. Bertseva, O. Naumenko, *J. Mol. Spectrosc.* 204 (2000) 94–105.
- [7] A. Jenouvrier, M.F. Mérienne, M. Carleer, R. Colin, A.-C. Vandaele, P.F. Bernath, O.L. Polyansky, J. Tennyson, *J. Mol. Spectrosc.* 209 (2001) 165–168.
- [8] A. Campargue, I. Vasilenko, O. Naumenko, *J. Mol. Spectrosc.* 234 (2005) 216–227.
- [9] V.V. Lazarev, T.M. Petrova, L.N. Sinita, Q.-S. Zhu, J.-X. Han, L.-Y. Hao, *Atmos. Oceanic Opt.* 11 (1998) 809–812.
- [10] S. Hu, H. Lin, S. He, J. Cheng, Q. Zhu, *Phys. Chem. Chem. Phys.* 1 (1999) 3727–3730.
- [11] O. Naumenko, S.-M. Hu, S.-G. He, A. Campargue, *Phys. Chem. Chem. Phys.* 6 (2004) 910–918.
- [12] M. Bach, S. Fally, P.-F. Coheur, M. Carleer, A. Jenouvrier, A.C. Vandaele, *J. Mol. Spectrosc.* 232 (2005) 341–350.
- [13] P. Theulé, A. Callegari, T.R. Rizzo, *J. Chem. Phys.* 122 (2005) 124312.
- [14] H. Partridge, D.W. Schwenke, *J. Chem. Phys.* 106 (1997) 4618–4639.
- [15] D.W. Schwenke, H. Partridge, *J. Chem. Phys.* 113 (2000) 6592–6597.
- [16] <<http://mark4sun.jpl.nasa.gov/data/spec/H2O/>> (26.02.2006).
- [17] L.S. Rothman, D. Jacquemart, A. Barbe, D. Chris Benner, M. Birk, L.R. Brown, M.R. Carleer, C. Chackerian Jr., K. Chance, L.H. Coudert, V. Dana, V.M. Devi, J.-M. Flaud, R.R. Gamache, A. Goldman, J.-M. Hartmann, K.W. Jucks, A.G. Maki, J.-Y. Mandin, S.T. Massie, J. Orphal, A. Perrin, C.P. Rinsland, M.A.H. Smith, J. Tennyson, R.N. Tolchenov, R.A. Toth, J. Vander Auwera, P. Varanasi, G. Wagner, *J. Quant. Spectrosc. Radiat. Transf.* 96 (2005) 139–204.
- [18] V.I. Zakharov, R. Imasu, K.G. Gribov, G. Hoffmann, J. Jouzel, *Geophys. Res. Lett.* 31 (2004) L12104.
- [19] M. Brouard, S.R. Langford, *J. Chem. Phys.* 106 (1997) 6354–6364.
- [20] P.-F. Coheur, S. Fally, M. Carleer, C. Clerbaux, R. Colin, A. Jenouvrier, M.-F. Mérienne, C. Hermans, A.C. Vandaele, *J. Quant. Spectrosc. Radiat. Transf.* 74 (2002) 493–510.
- [21] S. Fally, P.-F. Coheur, M. Carleer, C. Clerbaux, R. Colin, A. Jenouvrier, M.-F. Mérienne, C. Hermans, A.C. Vandaele, *J. Quant. Spectrosc. Radiat. Transf.* 82 (2003) 119–132.
- [22] M.-F. Mérienne, A. Jenouvrier, M. Carleer, P.-F. Coheur, R. Colin, S. Fally, C. Hermans, A.C. Vandaele, M. Bach, *J. Quant. Spectrosc. Radiat. Transf.* 89 (2003) 99–118.
- [23] M. Carleer, Wspectra: a Windows program to measure accurately the line intensities of high resolution Fourier Transform spectra, in: J.E. Russell, K. Schaefer, O. Lado-Bordowski (Eds.), *SPIE Proceedings of Series: Remote Sensing of Clouds and the Atmosphere V*, vol. 4168, 2001, pp. 337–342.
- [24] A.J. Hewitt, N. Doss, N.F. Zobov, O.L. Polyansky, J. Tennyson, *Mon. Not. R. astr. Soc.* 356 (2005) 1123–1126.
- [25] O. Naumenko, M. Sneep, M. Tanaka, S.V. Shirin, W. Ubachs, J. Tennyson, *J. Mol. Spectrosc.* 237 (2006) 63–69.
- [26] A.D. Bykov, O.V. Naumenko, A.M. Pshenichnikov, L.N. Sinita, A.P. Shcherbakov, *Opt. Spectrosc.* 93 (2003) 528–537.
- [27] D.W. Schwenke, private communication (2000).
- [28] S.S. Voronina, *Atmos. Oceanic Opt.* 15 (2002) 727–729.
- [29] S.A. Tashkun, private communication (2006).
- [30] J. Tennyson, G.J. Harris, R.J. Barber, S. La Delfa, B.A. Voronin, B.M. Kaminsky, Ya.V. Pavlenko, *Mol. Phys.* 105 (2007) 701–714.
- [31] J. Tennyson, M.A. Kostin, P. Barletta, G.J. Harris, J. Ramanlal, O.L. Polyansky, N.F. Zobov, *Computer Phys. Comm.* 163 (2004) 85–116.
- [32] O.N. Ulenikov, S.-M. Hu, E.S. Bekhtereva, G.A. Onopenko, X.-H. Wang, S.-G. He, J.-J. Zheng, Q.-S. Zhu, *J. Mol. Spectrosc.* 208 (2001) 224–235.
- [33] P. Macko, D. Romanini, S.N. Mikhailenko, O.V. Naumenko, S. Kassi, A. Jenouvrier, V.I. Tyuterev, A. Campargue, *J. Mol. Spectrosc.* 227 (2004) 90–108.
- [34] O.V. Naumenko, S. Voronina, S.-M. Hu, *J. Mol. Spectrosc.* 227 (2004) 151–157.
- [35] O. Naumenko, O. Leshchishina, A. Campargue, *J. Mol. Spectrosc.* 236 (2006) 58–69.
- [36] G. Li, H. Guo, *J. Mol. Spectrosc.* 210 (2001) 90–97.
- [37] N.F. Zobov, S.V. Shirin, O.L. Polyansky, J. Tennyson, P.-F. Coheur, P.F. Bernath, M. Carleer, R. Colin, *Chem. Phys. Lett.* 414 (2005) 193–197.
- [38] S.E. Choi, J.C. Light, *J. Chem. Phys.* 97 (1992) 7031–7054.
- [39] A. Bykov, O. Naumenko, L. Sinita, B. Voronin, J.-M. Flaud, C. Camy-Peyret, R. Lanquetin, *J. Mol. Spectrosc.* 205 (2001) 1–8.
- [40] P.-F. Coheur, P.F. Bernath, M. Carleer, R. Colin, O.L. Polyansky, N.F. Zobov, S.V. Shirin, J. Barber, J. Tennyson, *J. Chem. Phys.* 122 (2005) 074307.
- [41] J.R. Fair, O. Votava, D.J. Nesbit, *J. Chem. Phys.* 108 (1998) 72–80.